




RESEARCH ARTICLE

A five-bar mechanism to assist finger flexion-extension movement: system implementation

Araceli Zapatero-Gutiérrez^{1,*} , Eduardo Castillo-Castañeda¹  and Med Amine Laribi² 

¹Centro de Investigación en Ciencia Aplicada y Tecnología Avanzada Unidad Querétaro, Instituto Politécnico Nacional, Querétaro, Querétaro 76090, México and ²Institut PPRIME, Département Génie Mécanique et Systèmes Complexes, Université de Poitiers, Poitiers 86073, France

*Corresponding author. E-mail: araceli_zapatero@hotmail.com

Received: 27 November 2021; **Revised:** 21 June 2022; **Accepted:** 20 July 2022; **First published online:** 1 September 2022

Keywords: five-bar mechanism, finger rehabilitation, rehabilitation devices

Abstract

The lack of specialized personnel and assistive technology to assist in rehabilitation therapies is one of the challenges facing the health sector today, and it is projected to increase. For researchers and engineers, it represents an opportunity to innovate and develop devices that improve and optimize rehabilitation services for the benefit of society. Among the different types of injuries, hand injuries occur most frequently. These injuries require a rehabilitation process in order for the hand to regain its functionality. This article presents the fabrication and instrumentation of an end-effector prototype, based on a five-bar configuration, for finger rehabilitation that executes a natural flexion-extension movement. The dimensions were obtained through the gradient method optimization and evaluated through Matlab. Experimental tests were carried out to demonstrate the prototype's functionality and the effectiveness of a five-bar mechanism acting in a vertical plane, where gravity influences the mechanism's performance. Position control using fifth-order polynomials with via points was implemented in the joint space. The design of the end-effector was also evaluated by performing a theoretical comparison, calculated as a function of a real flexion-extension trajectory of the fingers and the angle of rotation obtained through an IMU. As a result, controlling the two degrees of freedom of the mechanism at several points of the trajectory assures the end-effector trajectory and therefore the fingers' range of motion, which helps for full patient recovery.

1. Introduction

The World Health Organization notes that rehabilitation is an essential part of universal health coverage. It predicts that the need for rehabilitation will increase worldwide due to changes in the health and characteristics of the population. It also points out that in some low- and middle-income countries, more than 50% of people do not receive the rehabilitation services they need. In addition, the rehabilitation services in 60-70% of countries have been negatively affected due to the COVID-19 pandemic [1].

The global rehabilitation needs remain unmet due to multiple factors, including the lack of qualified professionals to provide rehabilitation services. The worldwide ratio is less than ten qualified professionals per million inhabitants. On top of this, there is a lack of assistive technology and specialized equipment [1].

The development of assistive technology, such as rehabilitation devices, is a broad field of research and development, which, reaching the clinical stages, help the needs of physical rehabilitation.

The need for physical rehabilitation can be due to a wide range of injuries. Hand injuries are among the most frequent and may require surgical and non-surgical medical attention. It should be noted that the hand represents one of the most important extremities of the upper limb, and mobility deficiencies may have a direct impact on people's quality of life [2, 3]. Part of the recovery of the functionality of the hand involves the movement of the fingers, and a common deficiency is the difficulty of the patient

to extend the fingers [4]. The continuous flexion and extension movement of the fingers has proven to be a functional exercise for the recovery of the hand [5, 6].

Hand rehabilitation devices can be classified, based on their interface with the user, into two categories: exoskeleton and end-effector types. Both categories have been shown to contribute substantially to the motor recovery of the fingers [3, 7–9]. Rehabilitation using robotic devices such as exoskeletons and end-effectors has already been shown to have higher percentages of hand recovery compared to traditional therapy [3]. The study carried out in ref. [3] concluded that, in terms of recovery, exoskeletons could contribute to reaching a higher percentage compared to end-effectors. The issue is that the number of exoskeleton-type studies, such as those presented in refs. [10–12], is much greater than the number of end-effectors, which implies that increasing the study and development of this kind of device can change that assumption.

Another issue is that hand rehabilitation has taken a backseat when full upper limb rehabilitation is involved. This leads to hand rehabilitation starting up to three weeks later. This is a critical stage where the patient should ideally start with gentle exercises to help strengthen the damaged area [3, 13]. It is imperative to design tools that therapists can use at the appropriate times in each stage of the rehabilitation process.

The five-bar mechanism has been well studied in the literature due to its great adaptability for several trajectories, which can be executed even at high speeds. Optimization of a five-bar mechanism used for pick-and-place operations at high speed is presented in ref. [14]; the goal of the optimization was to minimize the root mean square torque of the actuators' torques for any trajectory defined. Using fifth-order polynomial motion profiles and defining the dexterous workspace, the selection of the configurations and trajectories for the computation of the mechanisms' electrostatic performance were chosen to obtain the shape of the five-bar links. Besides, the authors present an optimization to reduce the mass of the links. A winding hybrid-driven cable parallel manipulator is presented in ref. [15], which uses three five-bar mechanisms as a part of the design. The five-bar mechanism is attached to the cables to position the end-effector through a pulley. The winding hybrid-driven cable parallel manipulator was built for precision tracking experiments. A haptic device for finger and hand rehabilitation is presented in ref. [16]. This development consists of the optimization of a five-bar mechanism using a non-linear programming algorithm; the lengths of the links were determined by finding the best fitting between a human finger workspace and the device workspace. In this development, the patient is allowed to move the wrist, and there is no hand subjection, which might not make it convenient in the early stages of the rehabilitation process.

The design of a finger rehabilitation mechanism that executes the flexion-extension movement was presented in ref. [17]. The mechanism is designed as an end-effector device that executes a passive flexion-extension movement on the patient's fingers for the early stage of treatment. The device does not focus on performing specific tasks related to particular activities of daily life, such as grasping objects or fine motor function. The goal of this paper is to present the prototype development and functionality of the design presented in ref. [17], as well as its instrumentation to execute a defined trajectory through its end-effector. The main contribution of this study includes the following: (1) Design and optimization of an end-effector device for finger rehabilitation, based on a five-bar mechanism and real finger trajectory; (2) Implementation of a control scheme that correlates the Cartesian frame of a real flexion-extension trajectory with the articular frame using five-order polynomials to ensure continuous position, velocity and acceleration profiles; (3) The effectiveness of the proposed prototype to follow a real trajectory of fingers' flexion-extension based on the rotational angles of the end-effector and the real trajectory; and (4) Contribute to the state of the art in the study of end-effector rehabilitation device that promotes motor plasticity.

The paper is structured as follows: Section 2 presents the conceptual proposal of the prototype design and the optimal dimensions calculated by an optimization algorithm. Section 3 presents the development of the prototype including the fabrication and instrumentation process. Section 4 presents the prototype's end-effector trajectory and the comparison between the theoretical rotation angle and the real rotation angle of the end-effector. Finally, in Section 5, the conclusions are presented.

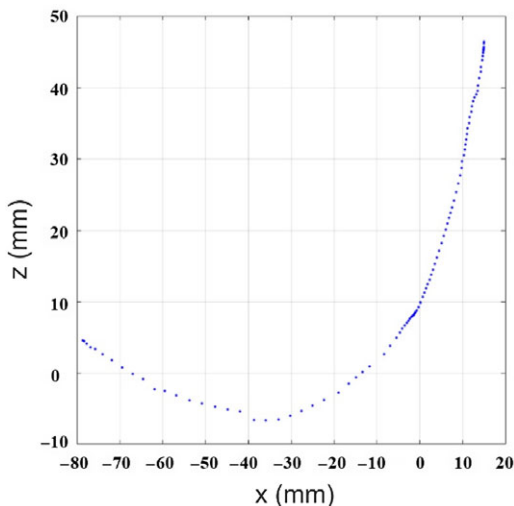


Figure 1. Real flexion-extension trajectory.

2. Conceptual prototype

The design of the prototype for rehabilitation of the flexion-extension movement of the fingers is based on the configuration of a five-bar mechanism. The five-bar mechanism has two degrees of freedom that allow it to generate different types of trajectories, a characteristic that makes it attractive for reproducing the natural flexion-extension movement of the fingers. The conceptual proposal of the design is explored in depth in ref. [17], where the optimal dimensions of the prototype were found through a gradient method. The results obtained in the previous work are briefly retaken in this article.

2.1. Desired trajectory

The desired trajectory for the end-effector corresponds to the natural flexion-extension movement of the fingers. As an end-effector mechanism, only the fingertip trajectory is considered. The development of the hand prototype presented in ref. [18] assures that the motion of the finger is performed with a typical motion, with this assumption it can be considered that an end-effector mechanism is enough to reproduce the finger movement.

A set of representative movement curves were obtained from a group of healthy subjects. It was possible to determine, through a principal component analysis, that the flexion-extension movement can be located within a plane, since there is minimal variation in one of the three coordinate axes. The representative curves for each finger vary in amplitude. The curve with the greatest amplitude (Fig. 1), which corresponds to the movement of the middle finger, is considered as the desired trajectory for this work [19]. The authors in ref. [20] found an important correlation ship among the index, middle, and thumb for rotational movement control of small objects; the results suggest that middle and thumb have a preponderant participation which can be a useful guide for designing new mechanisms.

Although only one curve is considered, the mechanism has been designed to modify the amplitude of the desired trajectory, as will be explained in Section 3.

2.2. Five-bar kinematic

The design of this rehabilitation device can be classified within the end-effector-type devices. Point C of a symmetric five-bar mechanism generates a natural flexion-extension trajectory of the fingers, when the actuated joints θ_1 and θ_2 move from θ_{1o} , θ_{2o} to θ_{1f} , θ_{2f} , respectively; as seen in Fig. 2(a).

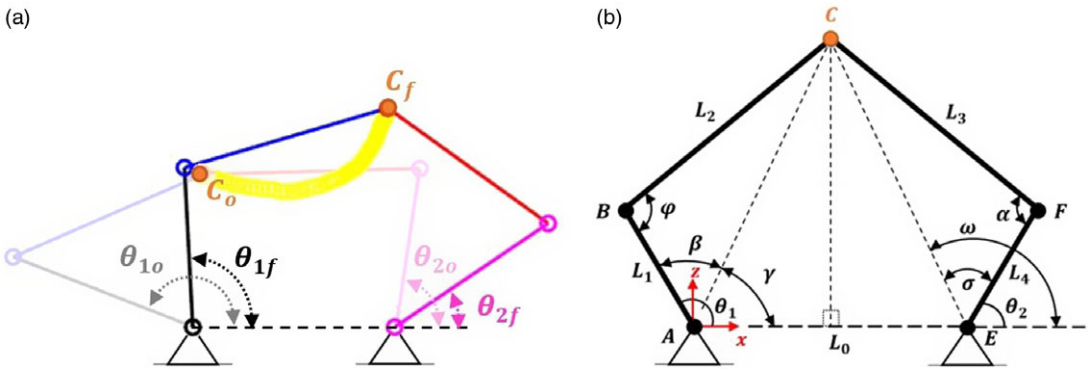


Figure 2. (a) Five-bar mechanism positions. (b) Five-bar mechanism configuration.

In Fig. 2(b), $L_1, L_2, L_3,$ and L_4 represent the lengths of the links, with $L_1 = L_4$ and $L_2 = L_3$. The length L_0 is the distance between the fixed points A and E . Point C is a rotational joint that joins the links L_2 and L_3 [17], its kinematic equation is given by Eq. (1) [21].

$$C = \begin{bmatrix} C_x \\ C_z \end{bmatrix} \tag{1}$$

where

$$C_x = L_1 \cos \theta_1 + \frac{1}{2} [L_0 + L_1(\cos \theta_2 - \cos \theta_1)] - [L_1(\sin \theta_2 - \sin \theta_1)] \left[\sqrt{\frac{L_2^2}{H^2} - \frac{1}{4}} \right]$$

$$C_z = L_1 \sin \theta_1 + \frac{1}{2} [L_1(\sin \theta_2 - \sin \theta_1)] + [L_0 + L_1(\cos \theta_2 - \cos \theta_1)] \left[\sqrt{\frac{L_2^2}{H^2} - \frac{1}{4}} \right]$$

$$H^2 = L_0^2 + 2L_0L_1(\cos \theta_2 - \cos \theta_1) + 2L_1^2 [1 - (\cos \theta_1 - \cos \theta_2)]$$

θ_1 is the sum of the angles β and γ as shown in Eq. (2), while the difference between the ω and σ angles compute θ_2 given by Eq. (3). The γ and ω angles come from the real flexion-extension trajectory as analyzed in ref. [17] and is shown in Fig. 1. The five-bar mechanism point C follows from i point to N point of the real trajectory expressed by D .

$$\theta_1 = \beta + \gamma \tag{2}$$

$$\theta_2 = \omega - \sigma \tag{3}$$

where

$$\gamma = \text{atan } 2(D_z, D_x)$$

$$\omega = \pi - \text{atan } 2(D_z, L_0 - D_x)$$

To obtain the angles β and σ , defined by Eqs. (4) and (5), it is necessary to calculate the φ and α angles. The φ and α angles are obtained by applying the law of cosines and the trigonometric properties of sine and cosine [21].

$$\beta = \text{atan } 2(L_2 \sin(\pi - \varphi), L_1 + L_2 \cos(\pi - \varphi)) \tag{4}$$

$$\sigma = \text{atan } 2(L_3 \sin(\pi - \alpha), L_4 + L_3 \cos(\pi - \alpha)) \tag{5}$$

Table I. Design vector *I* values.

<i>I</i> (mm)			Input angles (degrees)			
<i>L</i> ₁	<i>L</i> ₂	<i>L</i> ₀	θ _{1o}	θ _{1f}	θ _{2o}	θ _{2f}
101.09	108.67	101.20	153.55	92.37	83.07	40.44

where

$$\varphi = \text{atan } 2(\sin \varphi, \cos \varphi)$$

with

$$\cos \varphi = \frac{L_1^2 + L_2^2 - (D_x^2 + D_z^2)}{2L_1L_2}$$

$$\sin \varphi = B\sqrt{1 - \cos^2 \varphi}$$

and

$$\alpha = \text{atan } 2(\sin \alpha, \cos \alpha)$$

with

$$\cos \alpha = \frac{L_3^2 + L_4^2 - [(L_0 - D_{x_{i:N}})^2 + D_{z_{i:N}}^2]}{2L_3L_4}$$

$$\sin \alpha = F\sqrt{1 - \cos^2 \alpha}$$

There are four possible configurations for a five-bar mechanism, depending on the configuration of its elbows *B* and *F*. The prototype presented in this document explores only one of the four configurations when elbows *B* and *F* are both up, and they are represented by a magnitude of positive one [17].

2.3. Five-bar optimal solution

The geometric parameters of the five-bar mechanism were obtained using an optimization algorithm based on the generation of the real flexion-extension trajectory (Fig. 1). An objective function, given by Eq. (6), is used to minimize the error function *E(I)* [17].

$$E(\mathbf{I}) = \frac{1}{N} \sum_{i=1}^N \sqrt{(C_{x_i} - D_{x_i})^2 + (C_{z_i} - D_{z_i})^2} \tag{6}$$

E(I) is defined as the sum of the squared root of the *i*th position of the desired trajectory and the coordinates of point *C*, which represents the end-effector of the mechanism, and it is computed by Eq. (1). Through the gradient method, implemented in MATLAB with the *fmincon* function, the optimal parameters of the design vector *I*, as summarized in Table I, were found. The values of the input angles, as summarized in Table I, were computed using the Eqs. (2) and (3) considering the first point of the real flexion-extension trajectory, given by Fig. 1, and the last point of the real flexion-extension trajectory.

The gradient method, also known as non-linear programming, is used to find the minimum of a scalar function of several variables that begin with an initial estimate [22]. A maximum of 150 iterations with 2000 allowed evaluations of the function were chosen. The iterative process to minimize the objective function considers an upper and lower limit for each component of the design vector *I*. The design vector provides the length of the links and the initial position angles for *L*₁ and *L*₄ [17].

The optimization problem considers four constraint equations, Eqs. (7a), (7b), (7c), (7d), that ensures viable solutions for H and guarantees that the position of the end-effector, described in Eq. (1), is within real numbers.

$$R_1 = \left| \frac{L_1^2 + L_2^2 - (D_{x_i:N}^2 + D_{z_i:N}^2)}{2L_1L_2} \right| < 1 \tag{7a}$$

$$R_2 = \left| \frac{L_3^2 + L_4^2 - [(L_0 - D_{x_i:N})^2 + D_{z_i:N}^2]}{2L_3L_4} \right| < 1 \tag{7b}$$

$$R_3 = |H_i| < 1 \tag{7c}$$

$$R_4 = \left| \sqrt{\frac{L_2^2}{H_i^2} - \frac{1}{4}} \right| < 1 \tag{7d}$$

The constraint Eqs. (7a)–(7b) ensures always to obtain a viable solution for the coordinates of the point C of the mechanism. These constraints are computed inside the optimization algorithm for every iteration which implies that the vector design not only provides the optimal dimensions of the mechanism but also ensures that these dimensions can pass for every point of the reference trajectory, avoiding singularities.

Especially, the constraint Eqs. (7c) and (7d) restrict the solution to ensure that only feasible values are taken; therefore, the imaginary part derived from C_x and C_z is zero. The algorithm only finds an optimal solution when the constraints are met. In this way, it is conditioned to the fact that the determinant of the Jacobian matrix is different from zero for the entire trajectory of the end-effector.

The design parameters obtained in Table I affect the mechanism’s performance since the dimensions of the links determine the position that the end-effector can reach, which is strictly related to the real flexion-extension trajectory. The set of points of the real trajectory with which the coordinates of the end-effector are computed define the workspace of the mechanism; it must be ensured that for each coordinate within the workspace, a singularity is not reached.

The input angle values were computed by evaluating the inverse kinematics and lengths of the links provided by the optimal solution.

3. Prototype development

This section describes the development of the five-bar prototype based on the values of the optimal design vector I . The purpose of the prototype is to evaluate the functionality of the design and check the tracking of the end-effector trajectory.

3.1. Design and assembly

The prototype has two similar five-bar mechanisms that act in parallel. One of the mechanisms works as a master mechanism because it moves directly through the motors attached to its links L_1 and L_4 . The second mechanism acts as a slave because it follows the movements of the master mechanism through guide bars and a connecting bar located at the junction of links L_2 and L_3 , as shown in Fig. 3. This bar also has the connections to adjust the length of the thimbles (Fig. 4). A pair of brackets have been designed for the motors and the slave mechanism to be able to fix them to a base.

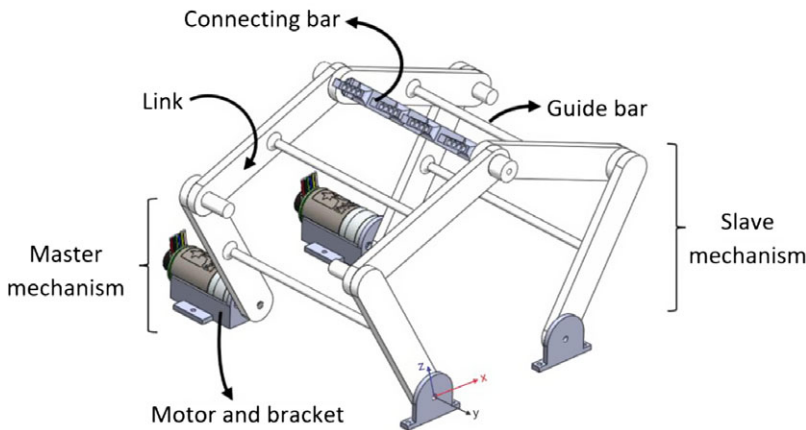


Figure 3. Rehabilitation prototype design.

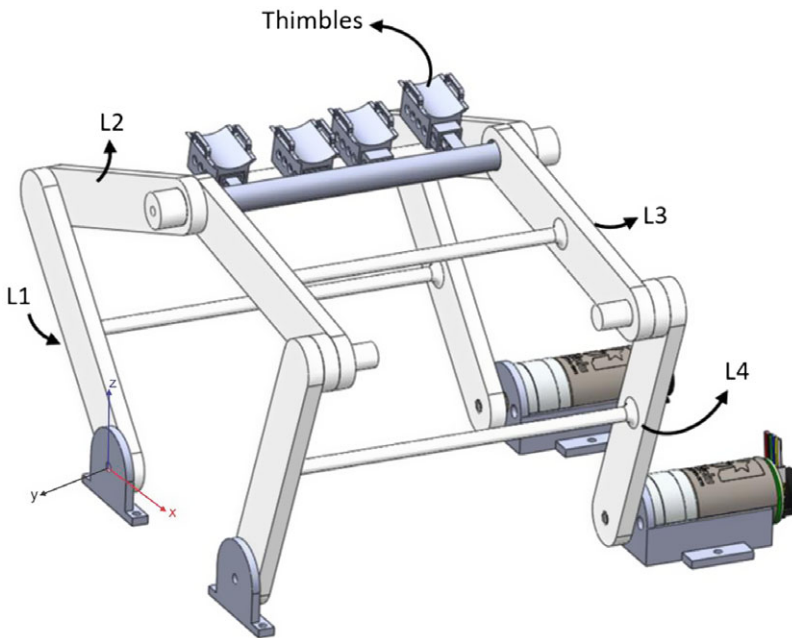


Figure 4. Rehabilitation prototype design, view with thimbles.

3.2. Materials, components, and control

The links of the mechanism are 6 mm thick and were printed in 3D using polylactic acid. The connecting bar, between the master mechanism and the slave mechanism, is designed to rotate freely to adapt to the position of the finger and has a diameter of 7 mm. Four 25 mm protruding bars are distributed along the connecting bar, which, in turn, are assembled with extension bars that allows the position of the thimbles to be adjusted (Fig. 5).

The prototype movement is executed using two 6V DC motors (Pololu, 34:1 Metal Gearmotor with 48 CPR Encoder) controlled via a RoboClaw 2x7A (Motion Control) control card. The control interface was carried out using LabView (National Instruments) running on a PC (Intel Core i5-6300HQ, 8.00 GB RAM, 2.30 GHz).

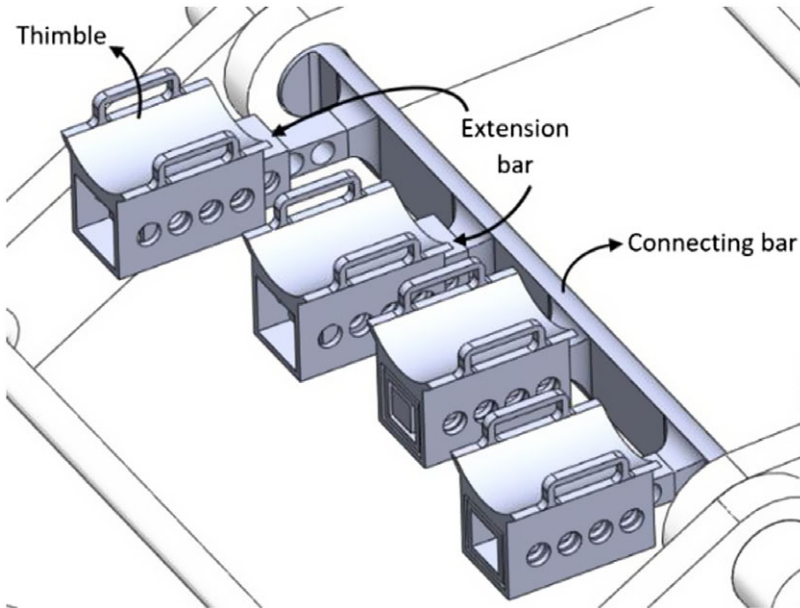


Figure 5. Connecting bar and thimbles adjustment.

The LabView program (VI) controls the motor via a point-to-point position control. A set of fifth-order polynomial, given by the set of Eqs. (8a)–(8e), generates the trajectory in a period of ten seconds. From Eq. (8a), i takes the value 1 for the motor M1 and 2 for the motor M2. The joint trajectory considers zero initial and final values for the velocities and accelerations of both motors, as well as two via points. Figure 6 shows the flowchart of the VI. The positions obtained through every encoder are received by an *Action-Status module*, which is integrated in the control card. The module compares the encoders' positions with the computed positions by the polynomials. A pair of subVIs (LabVIEW subprograms) contains the position equations given by (8b) and (8f). There is one subVI for every motor due to the different coefficients of the polynomials of each one. The coefficients of the polynomials represent the inputs of the block, and the desired position is the out. For simplicity, the value of the coefficients was obtained by MATLAB and added to the subVIs as constants. The output changes depending on the elapsed time, programmed from 0 to 10 s. The baud rate is 9600 and a 100-ms data reading-writing delay.

Fifth-order polynomials were chosen for the trajectory in the joint space to ensure continuity in position, velocity, and acceleration [23]. Equations (8e) and (8i) correspond to the rate of change of acceleration (jerk); computing the jerk can assure a smooth movement and allows to obtain the coefficients of the polynomials.

The design of the rehabilitation mechanism considers that the movement of the fingers starts from the flexed finger position to the extended finger position. In this article, a *cycle* is defined as the finger trajectory from the flexion position to the extended position and vice versa. In such a way, the trajectory begins and ends in the zero position as shown in Fig. 7.

$$\theta_{Mi}(t) = \begin{cases} \theta_{1i}(t) & \text{if } 0 \leq t \leq t_{v1} \\ \theta_{2i}(t) & \text{if } t_{v1} \leq t \leq t_{f1} \\ \theta_{3i}(t) & \text{if } t_{f1} \leq t \leq t_{v2} \\ \theta_{4i}(t) & \text{if } t_{v2} \leq t \leq t_{f2} \end{cases} \quad (8a)$$

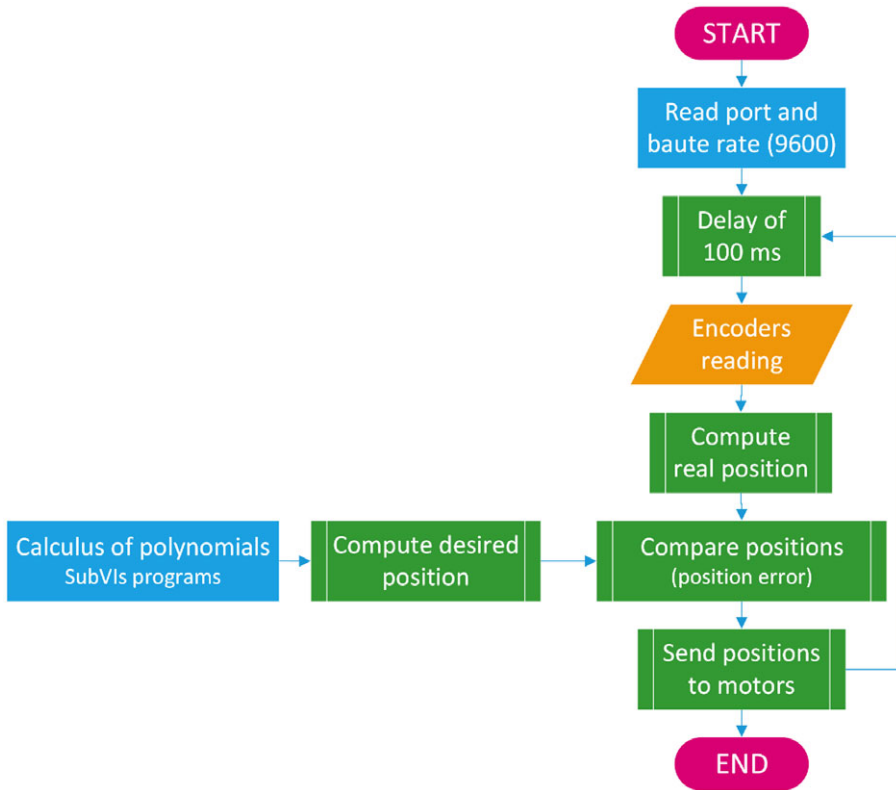


Figure 6. Flowchart of the LabView programming.

For $k \in \{1, 2\}$:

$$\theta_{ki}(t) = a_{0ki} + a_{1ki}t + a_{2ki}t^2 + a_{3ki}t^3 + a_{4ki}t^4 + a_{5ki}t^5 \tag{8b}$$

$$\dot{\theta}_{ki}(t) = a_{1ki} + 2a_{2ki}t + 3a_{3ki}t^2 + 4a_{4ki}t^3 + 5a_{5ki}t^4 \tag{8c}$$

$$\ddot{\theta}_{ki}(t) = 2a_{2ki} + 6a_{3ki}t + 12a_{4ki}t^2 + 20a_{5ki}t^3 \tag{8d}$$

$$\dddot{\theta}_{ki}(t) = 6a_{3ki} + 24a_{4ki}t + 60a_{5ki}t^2 \tag{8e}$$

and, where $k \in \{3, 4\}$:

$$\theta_{ki}(t) = b_{0ki} + b_{1ki}t + b_{2ki}t^2 + b_{3ki}t^3 + b_{4ki}t^4 + b_{5ki}t^5 \tag{8f}$$

$$\dot{\theta}_{ki}(t) = b_{1ki} + 2b_{2ki}t + 3b_{3ki}t^2 + 4b_{4ki}t^3 + 5b_{5ki}t^4 \tag{8g}$$

$$\ddot{\theta}_{ki}(t) = 2b_{2ki} + 6b_{3ki}t + 12b_{4ki}t^2 + 20b_{5ki}t^3 \tag{8h}$$

$$\dddot{\theta}_{ki}(t) = 6b_{3ki} + 24b_{4ki}t + 60b_{5ki}t^2 \tag{8i}$$

Considering that, for $k = 1$:

$$\theta_{ki}(t_{v1}) = \theta_{(k+1)i}(t_{v1}) \tag{8j}$$

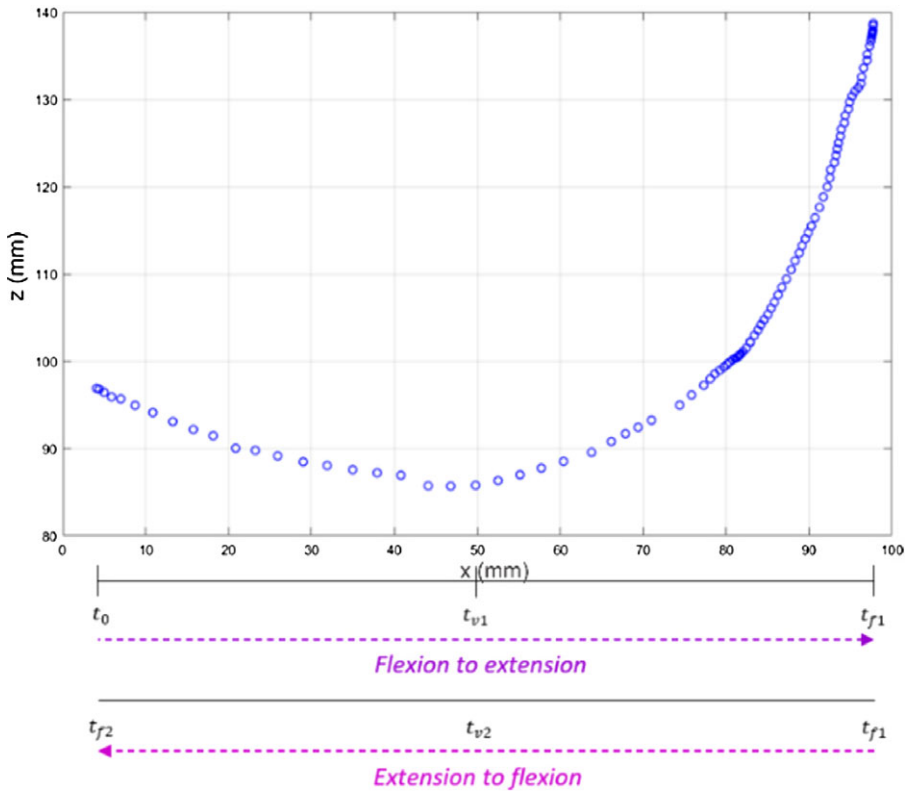


Figure 7. A cycle of movement.

$$\dot{\theta}_{ki}(t_{v1}) = \dot{\theta}_{(k+1)i}(t_{v1}) \tag{8k}$$

$$\ddot{\theta}_{ki}(t_{v1}) = \ddot{\theta}_{(k+1)i}(t_{v1}) \tag{8l}$$

and for $k = 3$:

$$\theta_{ki}(t_{v2}) = \theta_{(k+1)i}(t_{v2}) \tag{8m}$$

$$\dot{\theta}_{ki}(t_{v2}) = \dot{\theta}_{(k+1)i}(t_{v2}) \tag{8n}$$

$$\ddot{\theta}_{ki}(t_{v2}) = \ddot{\theta}_{(k+1)i}(t_{v2}) \tag{8o}$$

The Eq. (8b) evaluated in $k = 1$ provides the flexion (zero) position to the first via point. The Eq. (8b) evaluated in $k = 2$ provides the position from the first via point to the extension (final) position of the finger. θ_{1i} and θ_{2i} correspond to the half of a cycle.

Equation (8g) evaluated in $k = 3$, expresses the movement from the extended position to the second via point. Finally, Eq. (8g) evaluated in $k = 4$ provides the position from the second via point to flexion position of the finger, completing a cycle.

The coefficients of the polynomials corresponding to the first half of the cycle (C_{fe}) are calculated by multiplying the inverse matrix $M_{z_{1i}}$ that considers Eqs. (8b)–(8i) by the vector of defined conditions q_{1i} , as shown in Eq. (9a).

$$[C_{fe}]_{12 \times 1} = [M_{z_{1i}}]_{12 \times 12}^{-1} [q_{1i}]_{12 \times 1} \tag{9a}$$

where

$$q_{1i} = \begin{bmatrix} \theta_{1i}(0) \\ \dot{\theta}_{1i}(0) \\ \ddot{\theta}_{1i}(0) \\ \ddot{\theta}_{1i}(0) \\ \theta_{1i}(t_{v1}) \\ \theta_{2i}(t_{v1}) \\ 0 \\ 0 \\ \theta_{2i}(t_{f1}) \\ \dot{\theta}_{2i}(t_{f1}) \\ \dot{\theta}_{2i}(t_{f1}) \\ \ddot{\theta}_{2i}(t_{f1}) \end{bmatrix}$$

The coefficients of the polynomials corresponding to the second half of the cycle (C_{ef}) are calculated by multiplying the inverse matrix $M_{z_{2i}}$ that considers Eqs. (8j)–(8q) by the vector of defined conditions q_{2i} , as shown in

Eq. (9b).

$$[C_{ef}]_{12 \times 1} = [M_{z_{2i}}]^{-1}_{12 \times 12} [q_{2i}]_{12 \times 1} \tag{9b}$$

where

$$q_{2i} = \begin{bmatrix} \theta_{3i}(t_{f1}) \\ \dot{\theta}_{3i}(t_{f1}) \\ \dot{\theta}_{3i}(t_{f1}) \\ \ddot{\theta}_{3i}(t_{f1}) \\ \ddot{\theta}_{3i}(t_{f1}) \\ \theta_{3i}(t_{v2}) \\ \theta_{4i}(t_{v2}) \\ 0 \\ 0 \\ \theta_{4i}(t_{f2}) \\ \dot{\theta}_{4i}(t_{f2}) \\ \dot{\theta}_{4i}(t_{f2}) \\ \ddot{\theta}_{4i}(t_{f2}) \end{bmatrix}$$

An MPU-6050 IMU was placed on the connecting bar to measure the end-effector angle on the coordinate axes through an Arduino UNO. The connection is independent of the motor control program; it means that it does not close the control chain because it is used as an external sensor to verify the behavior of the connecting bar. The prototype instrumentation is shown in Fig. 8.

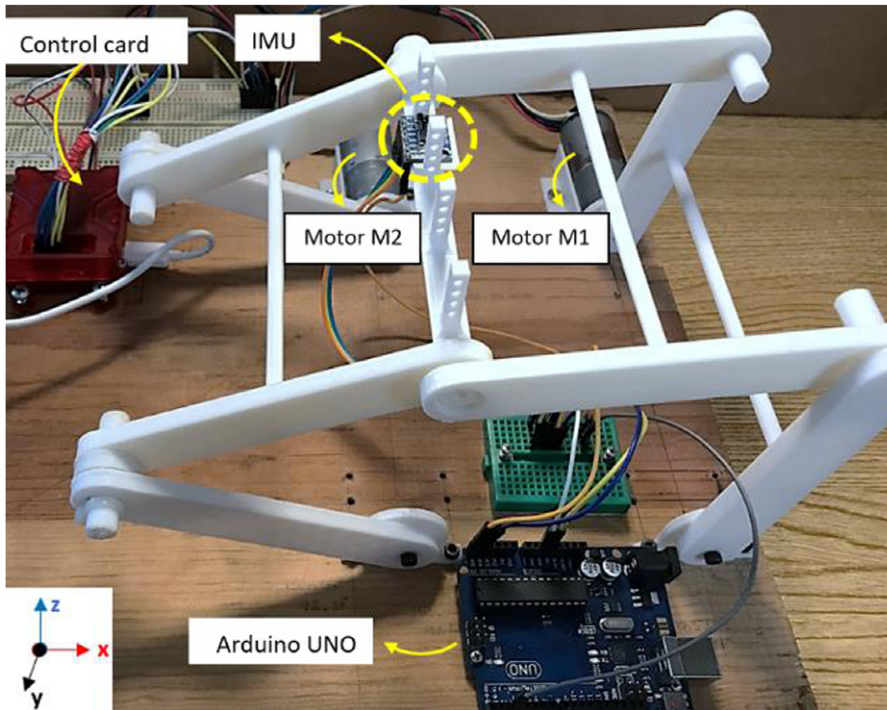


Figure 8. Mechanism instrumentation.

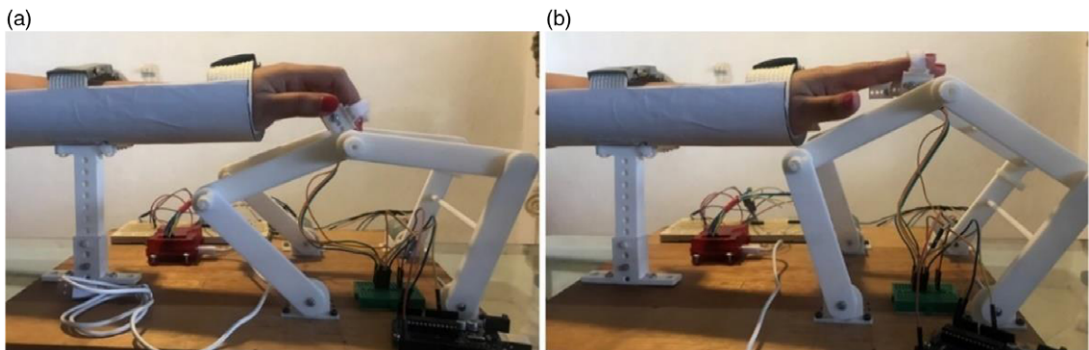


Figure 9. (a) Finger flexed position. (b) Finger extended position.

3.3. Experimental evaluation

To use the mechanism, the patient must sit in front of it and place his/her arm on the fixed forearm support. The arm is tied through a pair of straps which restricts wrist movement, as shown in Fig. 9. The fingers are tied to the thimbles in a flexed position. The trajectory along which the mechanism will guide the fingers begins with the flexed position and ends in the extended position.

The movement begins once the therapist initiates the movement cycle from a computer screen running the VI. If the therapist needs to stop the mechanism in any part of the trajectory, he/she can also do it from the VI. The hand position does not change while the mechanisms guide the finger through the desired trajectory. Figure 9 is only a representation; no hand experiments have been performed using the mechanism.

The flexion-extension trajectory is carried in ten seconds and represents one cycle of motion. The encoders were initialized to zero for 153° in the L_1 link connected to the M_2 motor, and 83° in the L_4 link

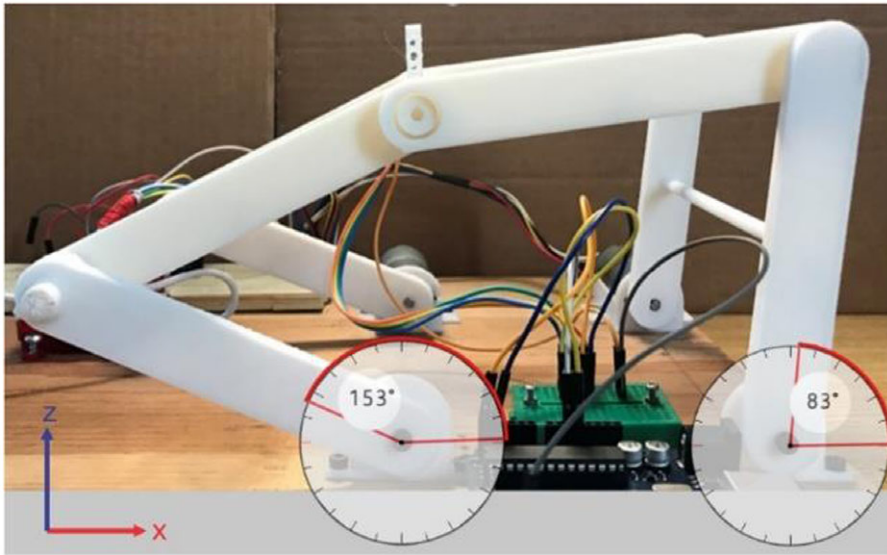


Figure 10. L_1 and L_4 links orientation.

connected to the M_1 motor, approximately, as shown in Fig. 10. The encoder resolution is 48.14 counts per turn at the output of the reducer. Table II indicates the relationship between the articular positions and the positions of the actuated links, at the initial, vias, and final points, obtained through inverse kinematics. The via points were computed for $t_{v1} = 2.5$ s and $t_{v2} = 7.5$ s. Figure 11 shows the profiles of the flexion-extension trajectory of both motors in radians.

The first experimentation step was to decouple the actuated links from the underactuated links. This made it possible to ensure that the range of motion of L_1 link and L_4 link will be consistent with the angles described by Table II. Once the range of movement of the actuated links corresponded to the desired movement, L_3 link and L_4 link were placed.

At the second experimentation step, the IMU was directly coupled to the connecting bar to measure the rotation of the bar with respect to the x , y , and z axes during four cycles. The connecting bar rotates freely and adjusts to the position of the finger as the mechanism performs the movement.

The angles obtained by the rotation of the IMU in the x axis (ζ_x), the y axis (ζ_y), and the z axis (ζ_z) during the four cycles are shown in Fig. 12. The IMU angles are given in degrees and represent the rotational position of the connecting bar, which in turn positions the fingers from flexion to extension and vice versa. It is worth mentioning that the displacement carried out by the connecting bar involves both a rotational movement in y axis and a translational movement in the xz plane. For this reason, it is to be expected that the greatest dispersion is found in the y axis, while the x and z axes show little rotational dispersion. It was observed that the connecting bar presents a little friction when rotating almost to the end of the trajectory.

The reason for using an IMU on the connector bar is because we are interested in measuring the rotation of the end-effector, and we suppose that this rotation could then be correlated with the rotation of the fingers and establish a pattern that helps measure the recovery of the patient. This assumption will be explored in future work.

4. Results

Figure 13 shows the different positions of the mechanism considering the via points while the mechanism is moving. Figure 14(a) shows the interpolation generated by these points and the estimated trajectory of point C.

Table II. Position setting.

Positions	Articular (encoder)	Links (degrees)
$\theta_{M1}(0)$	0	83.07
$\theta_{M1}(2.5)$	201	35.99
$\theta_{M1}(5)$	155	40.44
$\theta_{M1}(7.5)$	201	35.99
$\theta_{M1}(10)$	0	83.07
$\theta_{M2}(0)$	0	153.55
$\theta_{M2}(2.5)$	379	104.39
$\theta_{M2}(5)$	277	92.37
$\theta_{M2}(7.5)$	379	104.39
$\theta_{M2}(10)$	0	153.55

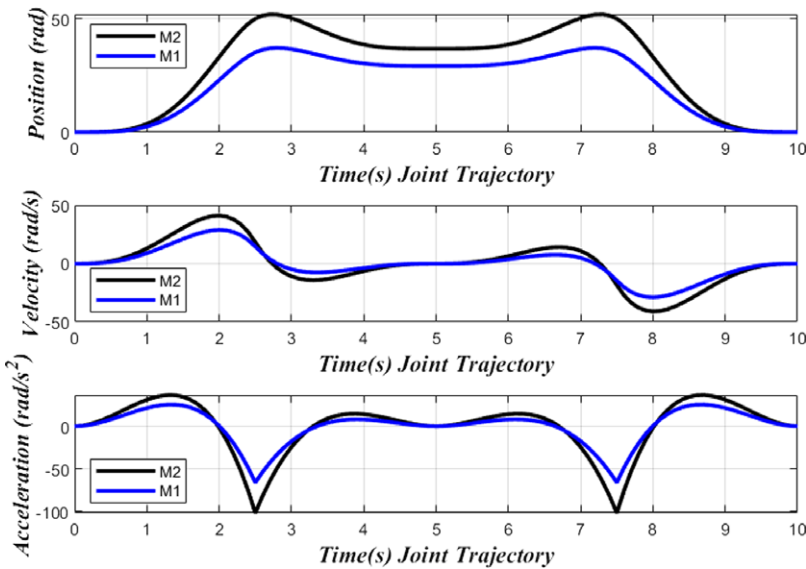


Figure 11. Joint movement profiles.

The angle of rotation obtained in the y axis through the IMU can be compared with the theoretical angle by considering the translation movement in the xz plane of the connection bar. The theoretical angle was obtained through Matlab. The inverse and direct kinematics of the mechanism are calculated using the optimal results of the gradient method (Section 2) [17] and the points generated by the desired trajectory of Fig. 1, considering a flexion-extension cycle.

With the coordinates of point C (C_x, C_z), a new vector V_{pi} is defined, V_{pi} change from the initial position from the i^{th} position. The V_p vector represents the relative position of two points, expressed by Eq. (10). The V_p vector joins two continuous points of the trajectory generated by the end-effector; the rectangular components V_r and V_q allow to calculate the theoretical angle ζ_{yTi} of the trajectory points through Eq. (11) according to the variation of the position, as shown in Fig. 14(b).

$$V_p = (C_{xi} - C_{xi-1}) \hat{i} + (C_{zi} - C_{zi-1}) \hat{k} = V_r \hat{i} + V_q \hat{k} \tag{10}$$

$$\zeta_{yT} = \text{atan} \left| \frac{V_q}{V_r} \right| \tag{11}$$

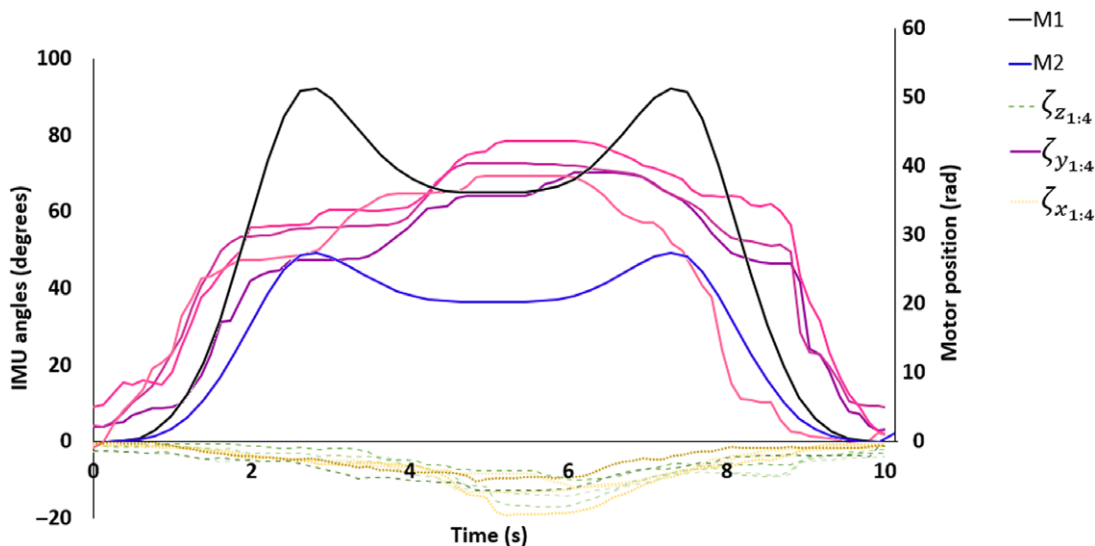


Figure 12. Comparison between the motor position and rotation angles obtained by the IMU.



Figure 13. Different positions of the mechanism.

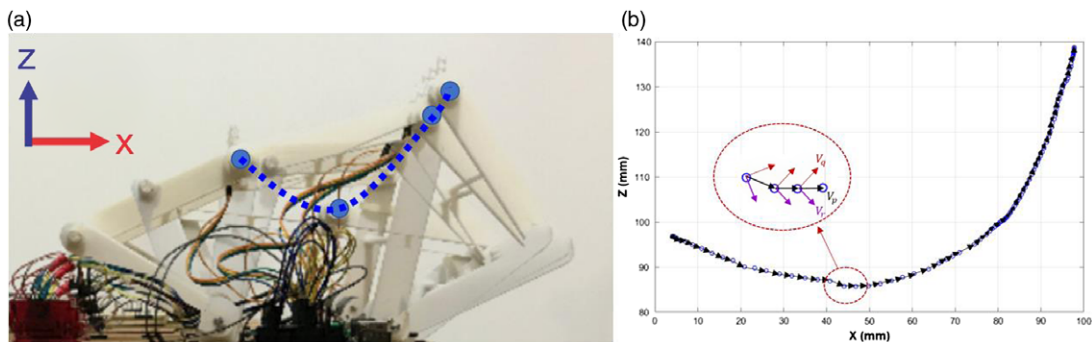


Figure 14. (a) Sequence of positions. (b) V_p vector.

The ζ_{yT} was computed only considering the movement from the flexion to extension position in order not to overwrite trajectory points. Figure 15(a) shows the theoretical angle obtained by the Eq. (11); in Fig. 15(b), the comparison among the theoretical angle with respect to the four cycles obtained with the IMU can be observed. For the purpose of comparison, an offset has been applied to each curve to start at angle zero in time zero. Figure 15(c) shows the error of each cycle with respect to the theoretical angle, and it is assumed that the friction presented by the connecting bar is directly related to the error.

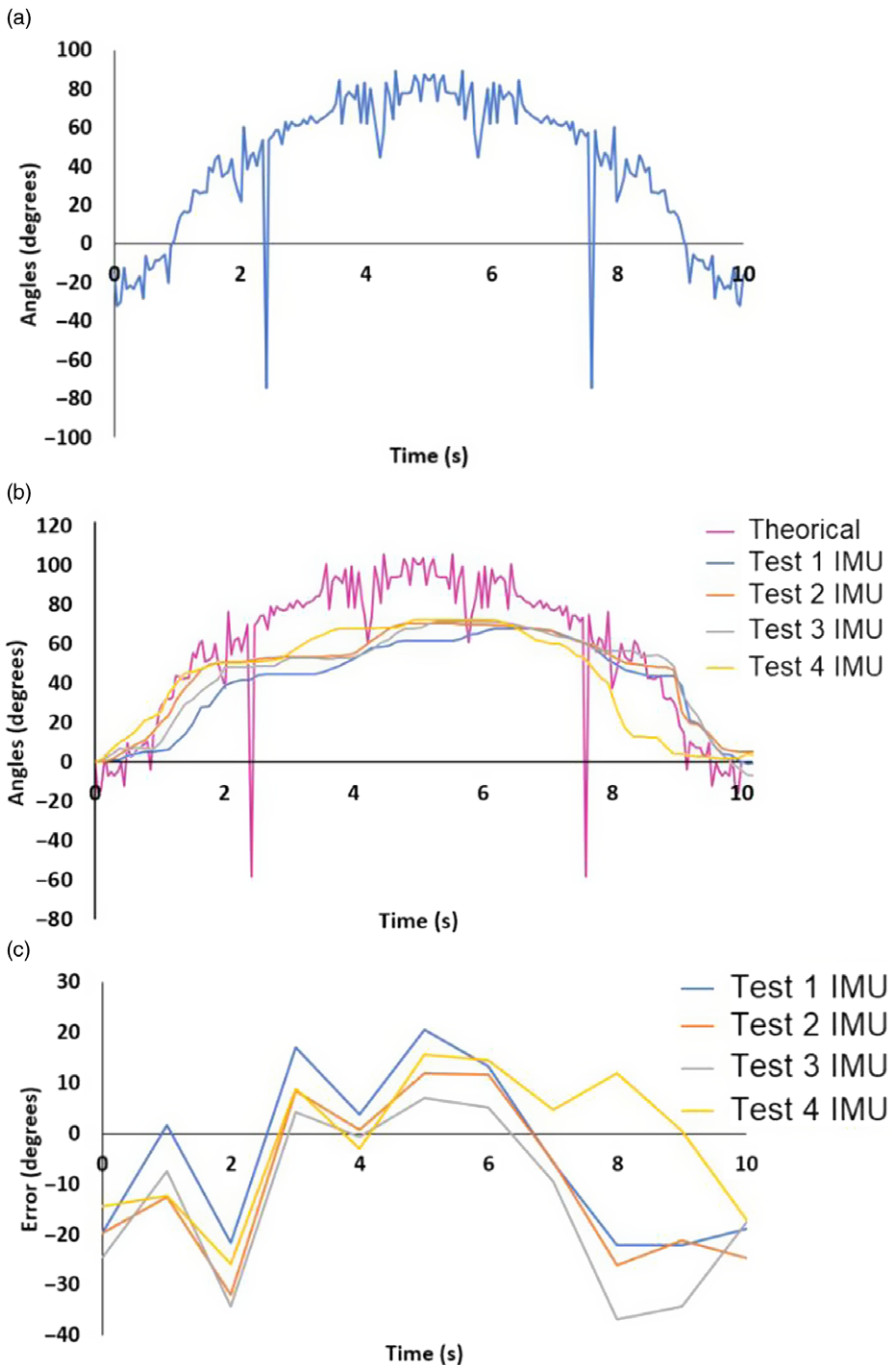


Figure 15. (a) Computed theoretical angle ζ_{yT} . (b) ζ_{yT} versus the four ζ_y obtained in the four cycles. (c) Error by cycle.

From Fig. 15(b), it can be observed that the theoretical value shows several peaks due to all the points of the desired trajectory are evaluated by the Eq. (11). Equation (11) considers only the tangent relation of the rectangular components. Instead, the graphs obtained by the IMU show a smoother behavior due to the IMU measurements considering the accelerometer and the gyroscope measurements, in addition to a complementary filter.

5. Discussion

The scope of this paper was to verify the proposal of an optimal five-bar mechanism to be used for hand rehabilitation support purposes. We fabricated the design proposed in ref. [17]; end-effector type designs have been less explored compared to exoskeleton-type designs, to claim that exoskeletons are more effective than end-effectors would be hasty. Increasing the type of end-effector devices is necessary to obtain a representative sample for comparison purposes.

From mechanism theory, it is well known that five-bar mechanisms have great versatility due to the workspace they can cover and the ability to reach high speeds. For hand rehabilitation purposes, the most attractive feature is that the five-bar mechanism can be configured to reach and generate complex trajectories, which makes it a good candidate for reproducing natural motion paths.

Experiments were carried out using an IMU to measure the rotation angle of the mechanism's end-effector to compare it with the real rotation of the finger, obtained from the analysis of a real flexion-extension trajectory. Instead of evaluating the performance of the device using only the characteristics of the movement profiles in the joint space, it was proposed to evaluate the performance by measuring the rotation of the end-effector to obtain a measure that would allow establishing a direct correlation with the rotation that it is produced from the flexion-extension movement of the finger.

We consider that being a device that will have direct contact with a human being, it is convenient to establish new experiments that allow defining the human-machine interaction process. From the experimentation carried out, related with the angle comparison, a significant error percentage between the one obtained by the IMU and the one calculated with the flexion-extension trajectory was found. Partly because the calculated theoretical angle considers all the points of the real finger trajectory, the curve used does not have any filter and some points are very close to others, influencing the tangent relationship. Also, gravity is a factor to be considered especially for the design of the links that are joined by the connecting bar. The weight of these links directly influences the tracking of the end-effector trajectory, and any misalignment affects the performance of the movement.

6. Conclusions

The design, manufacture and testing of an end-effector type prototype for the rehabilitation of fingers were presented. It is based on the configuration of an optimal five-bar mechanism, with optimal dimensions founded by an optimization algorithm, and two degrees of freedom. It was made using 3D printing and controlled using the joint space by fifth-order polynomials.

Regarding the design of the prototype, several points of improvement were observed and will be explored in the evolution of this project. Gravity is a factor that influences movement, although the mechanism is capable of following the points of the trajectory in the plane; the choice of the xz plane represents a challenge regarding the weight of the links; it was observed that after several tests the desired position tends to be lost due to the elbows (points B and D) falling.

The friction in the rotational articulation that carries the connecting bar may be reduced with the use of a bearing. The friction problem influences the measurement of the rotational angle and the finger range of motion.

Regarding the control loop, it was observed conveniently to add more via points to avoid undesired movements. Two degrees of freedom imply that it is necessary to assure the position relation between the motors, to obtain a coordinate joint trajectory that guarantees the end-effector trajectory.

Future work will consider the following aspects:

1. The study of the correlation between the angle of rotation of the end-effector and the rotation of the finger joints, in order to establish or discard patterns that allow measuring the progress of rehabilitation.
2. A protection mechanism in case of mechanical failure.
3. The study and analysis of materials applicable to medical device regulations.

4. The development of a mechanism-patient interaction control algorithm.

As far as the aforementioned aspects are covered, the patient's security will be improved.

Acknowledgments. The authors are grateful to the Instituto Politécnico Nacional, México and University of Poitiers, France; for the facilities provided for this research.

Financial support. This research received no external funding.

Conflicts of interest. The authors declare no conflict of interest.

Ethical considerations. None.

Authors' contributions. A.Z.G., M.A.L. and E.C.C. conceived and designed the study. A.Z.G. and M.A.L. conducted data gathering. A.Z.G. performed statistical analyses. A.Z.G. wrote the original draft preparation. M.A.L., E.C.C. and A.Z.G. reviewed and edited the article.

References

- [1] WHO Rehabilitation. Available at: <https://www.who.int/news-room/fact-sheets/detail/rehabilitation>.
- [2] C. S. Crowe, B. B. Massenburg, S. D. Morrison, J. Chang, J. B. Friedrich, G. G. Abady, F. Alahdab, V. Alipour, J. Arabloo, M. Asaad, M. Banach, A. Bijani, A. M. Borzi, N. I. Briko, C. D. Castle, D. Y. Cho, M. T. Chung, A. Daryani, G. T. Demoz, Z. V. Dingels, H. T. Do, F. Fischer, J. T. Fox, T. Fukumoto, A. K. Gebre, B. Gebremichael, J. A. Haagsma, A. Haj-Mirzaian, D. W. Handiso, S. I. Hay, C. L. Hoang, S. S. N. Irvani, J. J. Jozwiak, R. Kalhor, A. Kasaeian, Y. S. Khader, R. Khalilov, E. A. Khan, R. Khundkar, S. Kisa, A. Kisa, Z. Liu, M. Majdan, N. Manafi, A. Manafi, A.-L. Manda, T. J. Meretoja, T. R. Miller, A. Mohammadian-Hafshejani, R. Mohammadpourhodki, M. A. Mohseni Bandpei, A. H. Mokdad, M. D. Naimzada, D. E. Ndwandwe, C. T. Nguyen, H. L. T. Nguyen, A. T. Olagunju, T. O. Olagunju, H. Q. Pham, D. R. Angga Pribadi, N. Rabiee, K. Ramezanzadeh, K. Ranganathan, N. L. S. Roberts, L. Roever, S. Safari, A. M. Samy, L. S. Riera, S. Shahabi, C.-G. Smarandache, D. O. Sylte, B. E. Tesfay, B. X. Tran, I. Ullah, P. Vahedi, A. Vahedian-Azimi, T. Vos, D. H. Woldeyes, A. B. Wondmieneh, Z.-J. Zhang and S. L. James, "Global trends of hand and wrist trauma: A systematic analysis of fracture and digit amputation using the global burden of disease 2017 study," *Inj. Prev.* **26**(Supp 1), i115–i124 (2020). doi: [10.1136/injuryprev-2019-043495](https://doi.org/10.1136/injuryprev-2019-043495).
- [3] L. Moggio, A. de Sire, N. Marotta, A. Demeco and A. Ammendiola, "Exoskeleton versus end-effector robot-assisted therapy for finger-hand motor recovery in stroke survivors: systematic review and meta-analysis," *Top. Stroke Rehabil.* (6), 1–12 (2021). doi: [10.1080/10749357.2021.1967657](https://doi.org/10.1080/10749357.2021.1967657).
- [4] P. Esmatloo and A. A. Deshpande, "Quality-Focused, Impairment-Targeted Approach in Rehabilitation of the Hand after Stroke," **In:** *Robot-aided Neuromechanic Workshop, 2020 IEEE RAS/EMBS International Conference on Biomedical Robotics & Biomechatronics (BIOROB 2020)* pp. 1–3.
- [5] J. R. Carey, T. J. Kimberley, S. M. Lewis, E. J. Auerbach, L. Dorsey, P. Rundquist and K. Ugurbil, "Analysis of fMRI and finger tracking training in subjects with chronic stroke," *Brain* **125**(4), 773–788 (2002).
- [6] J. R. Carey, W. K. Durfee, E. Bhatt, A. Nagpal, S. A. Weinstein, K. M. Anderson and S. M. Lewis, "Comparison of finger tracking versus simple movement training via telerehabilitation to alter hand function and cortical reorganization after stroke," *Neurorehabil. Neural. Repair* **21**(3), 216–232 (2007). doi: [10.1177/1545968306292381](https://doi.org/10.1177/1545968306292381).
- [7] Z. Yue, X. Zhang and J. Wang, "Hand rehabilitation robotics on poststroke motor recovery," *Behav. Neurol.* **2017**(3), 1–20 (2017). doi: [10.1155/2017/3908135](https://doi.org/10.1155/2017/3908135).
- [8] J. Stein, L. Bishop, G. Gillen and R. Helbok, "Robot-assisted exercise for hand weakness after stroke: A pilot study," *Am. J. Phys. Med. Rehabil.* **90**(11), 887–894 (2011). doi: [10.1097/PHM.0b013e3182328623](https://doi.org/10.1097/PHM.0b013e3182328623).
- [9] P. Wardhani, I. Triyani, F. Ardiansyah and F. A. de Matos, "Finger exoskeleton in simple motor rehabilitation therapy on arm and hand muscle ability of post-stroke sufferers," *J. Inf. Kesehatan* **19**(1), 1–11 (2021). doi: [10.31965/infokes](https://doi.org/10.31965/infokes).
- [10] I. Ertas, E. Hocaoglu and V. Patoglu, "AssistOn-Finger: An under-actuated finger exoskeleton for robot-assisted tendon therapy," *Robotica* **32**(8), 1363–1382 (2014). doi: [10.1017/S0263574714001957](https://doi.org/10.1017/S0263574714001957).
- [11] H. Talat, H. Munawar, H. Hussain and U. Azam, "Design, modeling and control of an index finger exoskeleton for rehabilitation," *Robotica*, 1–25 (2022). doi: [10.1017/S0263574722000388](https://doi.org/10.1017/S0263574722000388).
- [12] S. Davarzani, M. A. Ahmadi-Pajouh and H. Ghafarirad, "Design of sensing system for experimental modeling of soft actuator applied for finger rehabilitation," *Robotica* **40**(7), 2091–2111 (2022). doi: [10.1017/S0263574721001533](https://doi.org/10.1017/S0263574721001533).
- [13] Acute/Sub-Acute/Chronic Stages. <https://www.cindyprocterrmt.com/acutesub-acutechronic-stages.html>.
- [14] S. Briot and A. Goldsztejn, "Topology optimization of industrial robots: Application to a five-bar mechanism," *Mech. Mach. Theory* **120**(2), 30–56 (2018). doi: [10.1016/j.mechmachtheory.2017.09.011](https://doi.org/10.1016/j.mechmachtheory.2017.09.011).
- [15] B. Zin, H. Sun and D. Zhang, "Design, analysis and control of a winding hybrid-driven cable parallel manipulator, robotics and computer," *Integr. Manuf.* **48**(2), 196–208 (2017). doi: [10.1016/j.rcim.2017.04.002](https://doi.org/10.1016/j.rcim.2017.04.002).

- [16] O. A. Daud, F. Biral, R. Oboe and L. Piron, "Design of a Haptic Device for Finger and Hand Rehabilitation," **In: IECON 2010 - 36th Annual Conference on IEEE Industrial Electronics Society** (2010) pp. 2075–2080. doi: [10.1109/IECON.2010.5675347](https://doi.org/10.1109/IECON.2010.5675347).
- [17] A. Zapatero-Gutiérrez, M. A. Laribi and E. Castillo-Castañeda, "Optimal Design of a Five-Bar Mechanism Dedicated to Assisting in the Fingers Flexion-Extension Movement," **In: Mechanism Design for Robotics**, (S. Zeghloul, M. A. Laribi and M. Arsicault, eds.), vol. 103 (Springer International Publishing, Cham 2021) pp. 256–264.
- [18] M. Ceccarelli, N. Rodríguez and G. Carbone, "Design and tests of a three finger hand with 1-DOF articulated fingers," *Robotica* **24**(2), 183–196 (2006). doi: [10.1017/S0263574705002018](https://doi.org/10.1017/S0263574705002018).
- [19] A. Zapatero-Gutiérrez, E. Castillo-Castañeda and M. A. Laribi, "On the optimal synthesis of a finger rehabilitation slider-crank-based device with a prescribed real trajectory: Motion specifications and design process," *Appl. Sci.* **11**(2), 1–24 (2021). doi: [10.3390/app11020708](https://doi.org/10.3390/app11020708).
- [20] M. Orlando, A. Dutta, A. Saxena, L. Behera, T. Tamei and T. Shibata, "Manipulability analysis of human thumb, index and middle fingers in cooperative 3D rotational movements of a small object," *Robotica* **31**(5), 797–809 (2013). doi: [10.1017/S0263574713000064](https://doi.org/10.1017/S0263574713000064).
- [21] G. He and Z. Lu, "Optimization of planar Five-bar parallel mechanism via Self-reconfiguration method," *Chin. J. Aeronaut.* **18**(2), 185–192 (2005).
- [22] The MathWorks, Inc., Optimization Toolbox for Use with MATLAB, User's Guide. Ver-sion 2 (1999-2000), pp. 4-32-4-44.
- [23] C. D. Porawagama and S. R. Munasinghe, "Reduced Jerk Joint Space Trajectory Planning Method using 5-3-5 Spline Cfor Robot Manipulators," **In: 7th International Conference on Information and Automation for Sustainability "Sharpening Futur with Sustain Technol ICIAfS 2014** (2014). doi: [10.1109/ICIAfS.2014.7069580](https://doi.org/10.1109/ICIAfS.2014.7069580).
- [24] G. Alici, "Determination of singularity contours for five-bar planar parallel manipulators," *Robotica* **18**(5), 569–575 (2000). doi: [10.1017/S0263574700002733](https://doi.org/10.1017/S0263574700002733).
- [25] cond, Condition Number of matrix. Matlab Documentation.
- [26] S. Zarkandi, "Isotropy analysis of spherical mechanisms using an instantaneous-pole based method, engineering science and technology," *Int. J.* **20**(1), 240–246 (2017). doi: [10.1016/j.jestch.2016.08.016](https://doi.org/10.1016/j.jestch.2016.08.016).

Appendix

The evaluation of the Jacobian matrix, given by Eq. (A1), helps to identify the kinematics performance of the mechanism. To obtain the coefficients of the Jacobian matrix, the differential equation given by (A2) must be solved, and the detailed solution can be found in ref. [21].

$$\mathbf{J} = -\mathbf{B}^{-1}\mathbf{A} \quad (\text{A1})$$

where

$$\mathbf{A} = \begin{bmatrix} a_{11} & a_{12} \\ a_{21} & a_{22} \end{bmatrix}, \mathbf{B} = \begin{bmatrix} b_{11} & b_{12} \\ b_{21} & b_{22} \end{bmatrix}$$

$$\mathbf{A}\dot{\theta}_M + \mathbf{B}\mathbf{X} = \mathbf{0} \quad (\text{A2})$$

where

$$\dot{\theta}_M = [\theta_1 \quad \theta_2]^T, \mathbf{X} = [\dot{c}_x \quad \dot{c}_z]^T$$

The evaluation of Jacobian matrix allows to determine the kind of singularity for closed-loop kinematic chains; the singularities can occur whenever the determinants of \mathbf{A} and/or \mathbf{B} are zero [24].

Besides, Eq. (A3) defines the condition number, used to analyze the performance of a five-bar mechanism [21]. The condition number is the ratio of the largest singular value of the Jacobian matrix to the smallest singular value [25] and satisfies the relationship $1.0 \leq C(\mathbf{J}) < \infty$ [21]. This relationship implies that when the condition number is close to 1.0, the mechanism reaches an isotropic configuration [26].

$$C(\mathbf{J}) = \|\mathbf{J}\| \cdot \|\mathbf{J}^{-1}\| \quad (\text{A3})$$